Chapter 11

Advanced Methods for Creep in Engineering Design

William Harrison, Mark Whittaker and
Veronica Gray

Additional information is available at the end of the chapter

http://dx.doi.org/10.5772/intechopen.72319

Abstract

There are many applications where the combination of stress and elevated temperature require creep to be considered during the design process. For some applications, an evaluation of rupture life for given conditions is sufficient, however, for components such as those in gas turbine aeroengines, the accumulation of creep strain over time and the effect this has on other phenomena, such as high-temperature fatigue must be considered. In this chapter, modern creep curve modelling methods are applied to alloys used in gas turbine applications over a wide range of test conditions. Also, different creep hardening modelling methods are discussed along with their application to transient creep showing the deficiencies of simplistic models. Models are related to micromechanical properties where possible, and creep damage models are evaluated and applied to different applications using finite element analysis (FEA).

Keywords: creep, creep damage, stress relaxation, finite element analysis (FEA)

1. Introduction

When designing components for high temperature applications, the effects of creep must be considered. For simple cases, prediction methods that evaluate creep rupture life, t_F, based on applied stress and temperature are sufficient. These 'single-point' prediction methods such as those proposed by Norton [1], Larson and Miller [2] and more recently, the hyperbolic tangent method [3] and Wilshire equations [4], vary in complexity and in their ability to predict creep properties of the full range of applied conditions [5, 6]. Similarly, minimum creep rates, $\dot{\varepsilon}_m$, can be related to applied stress and temperature using similar equations or by using the Monkman-Grant relationship [7],

$$M = t_F \dot{\varepsilon}_m \tag{1}$$

where M is the Monkman-Grant constant. The minimum creep rate, although useful for simple calculations, does not represent the full range of creep behaviour for an alloy at any given

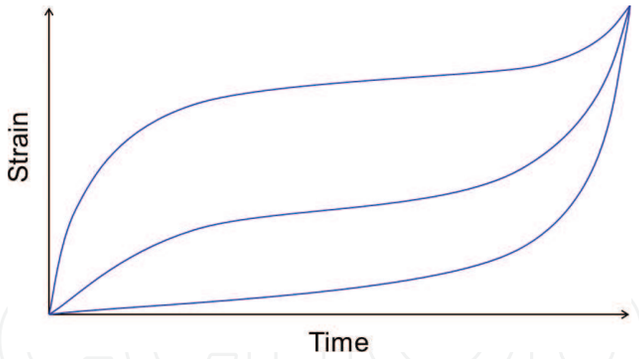

Figure 1. Schematic representation of different creep curves with equivalent rupture times and minimum creep rates.

applied conditions. On applying load to a material at high temperature the initial creep rate is high before decreasing to a minimum rate, a phenomenon known as primary creep. As deformation continues, the creep rate increases to failure during tertiary creep, giving the creep curve the characteristic shape shown in **Figure 1**. The shape of a creep curve can vary significantly depending on material and applied conditions [8]. This can have a considerable influence when calculating the lives of engineering components, especially in components where the effects of creep deformation and damage interact with other phenomenon such as fatigue during high-temperature fatigue or thermomechanical fatigue (TMF) [9].

Evaluating creep behaviour based on single point prediction methods alone cannot fully describe the shape of a creep curve since different curves can exhibit the same rupture life and minimum creep rate (**Figure 1**). Furthermore, to evaluate the creep behaviour of complex shaped components, simple calculations must be replaced by a more multifaceted approach such as finite element analysis [10]. To develop creep models suitable for finite element analysis, the full creep curve of a material must be obtainable over a wide range of conditions and an appropriate hardening model must be used. Furthermore, in order to predict rupture during variable creep conditions, a suitable damage model must be used.

2. Creep deformation

2.1. Full creep curve prediction methods

Many approaches exist for evaluating creep deformation behaviour from simple time-hardening models which only predict tertiary creep, to phenomenological models which aim to predict the micro-mechanisms of creep. Two main approaches for predicting full creep curves are investigated in this section. The first approach involves evaluating the times to given creep strain levels for a range of tests using a similar approach to stress rupture. Parameters are then derived to describe how this relationship varies with increasing creep strain. Examples of this method include an empirical relationship proposed by Gray and Whittaker [11] and a method based on the Wilshire equations [12, 13]. The former method relates times to strain, t_ε, to applied test conditions using

$$t(\varepsilon)\exp\left(\frac{-Q_c^*}{RT}\right) = M(\varepsilon)\left(1-\frac{\sigma}{\sigma_N}\right)^{P(\varepsilon)} \tag{2}$$

where the σ_N is the temperature dependent tensile strength, yield stress or proof stress. The parameters $M(\varepsilon)$ and $P(\varepsilon)$ are related to strain using a Frechet and Lognormal distribution with μ = 0, respectively

$$M(\varepsilon) = A_1 \exp\left(-\left(\frac{\varepsilon}{A_2}\right)^{-A_3}\right) \tag{3}$$

$$P(\varepsilon) = \frac{A_4}{\varepsilon A_5\sqrt{2\pi}} \exp\left(-\frac{\left[\ln\left(A_6\varepsilon\right)\right]^2}{2A_5^2}\right) + A_7 \tag{4}$$

where A_{1-7} are material constants, derived from experimental data. This method has been successfully applied to many creep resistant metals and alloys [11].

The Wilshire approach has been show to extrapolate stress rupture times and minimum creep rates well [4, 5, 12–15]. An extension of this method uses an equation of similar form to relate times to a given creep strain to applied stress and temperature,

$$\frac{\sigma}{\sigma_{\mathrm{TS}}} = \exp\left\{-k_3\left[t_\varepsilon \exp\left(\frac{-Q_c^*}{RT}\right)\right]^w\right\} \tag{5}$$

where σ and T are the applied test stress and temperature respectively, t_ε is the time to a given creep strain, σ_{TS} is the ultimate tensile strength at applied test temperature, and, Q_c^* is the activation energy for creep evaluated for $1/T$ against $\sigma/\sigma_{\mathrm{TS}}$. The material constants k_3 and w are obtained from the gradient and intercept from plotting $\ln\left(\ln\left(\sigma/\sigma_{\mathrm{TS}}\right)\right)$ against $t_\varepsilon \exp\left(-Q_c^*/RT\right)$. Eq. (5) has been successfully used to represent creep data for alloys such as Ti834 [12] and Alloy720Li [13]. **Figure 2** shows creep strain data for Inconel100 with Eq. (5) representing creep strain data from 0.05 to 2% creep strain. Values for k_3 and w and in some cases Q_c^*, are not always constant across the full range of creep conditions. Studies [13, 14] have shown that in the case of creep rupture, there may be 2 or more sets of these parameters to account for different dominant creep mechanisms at different applied conditions. These changes in parameters usually occur at phenomena such as above and below the yield stress where dislocation networks change considerably [15]. Similar 'break points' have been observed for predicted times to strain for the nickel based superalloy, Alloy720Li [13].

Different relationships have been proposed to relate the parameters of Eq. (5) for different values of strain. For the nickel based superalloy Alloy720Li, w was found to vary minimally as strain increased and was assumed to be constant. A power law relationship was used to relate k_3 to creep strain, ε:

$$k_3 = k_{3,0} + k_{3,1}\varepsilon^{-k_{3,2}} \tag{6}$$

where $k_{3,0}$, $k_{3,1}$ and $k_{3,2}$ are material constants obtained from experimental data [13]. Care must be taken when evaluating the trends in w and k_3 because negative creep rates are possible if they deviate significantly with test data.

An alternative method to predicting full creep curves involves using equations to represent time verses creep strain behaviour and relating the parameters of these equations to applied

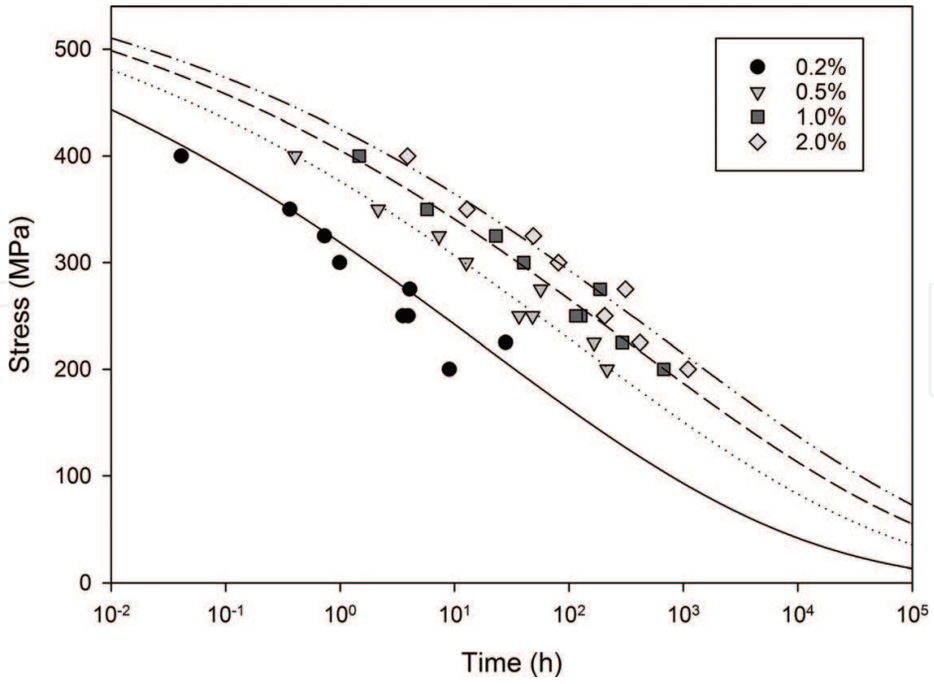

Figure 2. Times to 0.2%, 0.5%, 1% and 2% strain for Inconel100 with fits obtained using Eq. (5).

stress and temperature. Examples of this method include the theta-projection method [16, 17], a model by Dyson and McLean [18], and, a true stress method proposed by Wu et al. [19]. Both methods split the creep curve in to primary and tertiary regions, using equations of similar form to characterise each region. In the case of the theta method, creep strain is related to time using:

$$\varepsilon = \theta_1\left(1 - e^{-\theta_2 t}\right) + \theta_3\left(e^{\theta_4 t} - 1\right) \tag{7}$$

where θ_{1-4} are the 4-θ coefficients obtained from the experimental test data. These parameters are determined by minimising ϕ in the expression:

$$\phi^{n-1} = \sum_{i=1}^{n-1}\left[\varepsilon_i - \theta_1\left(1 - e^{-\theta_2 t_i}\right) + \theta_3\left(e^{\theta_4 t_i} - 1\right)\right]^2 \tag{8}$$

for n data points where ε_i and t_i are strain and time values for each data point. The expression $\theta_1\left(1 - e^{-\theta_2 t}\right)$ represents the decreasing rate of primary creep and $\theta_3\left(e^{\theta_4 t} - 1\right)$ represents tertiary creep. The parameters θ_1 and θ_3 represent the magnitude of primary and tertiary creep respectively and are referred to as scale parameter, whereas θ_2 and θ_4 characterise the curvature of the primary and tertiary phases and are termed rate parameters (**Figure 3**). **Figure 4** shows how this method has been used to accurately represent the curve shapes of many different metals and alloys over a range of applied conditions.

Various methods have been proposed to relate θ_{1-4} to applied test conditions. Evans [17] used a multi-linear approach whereby:

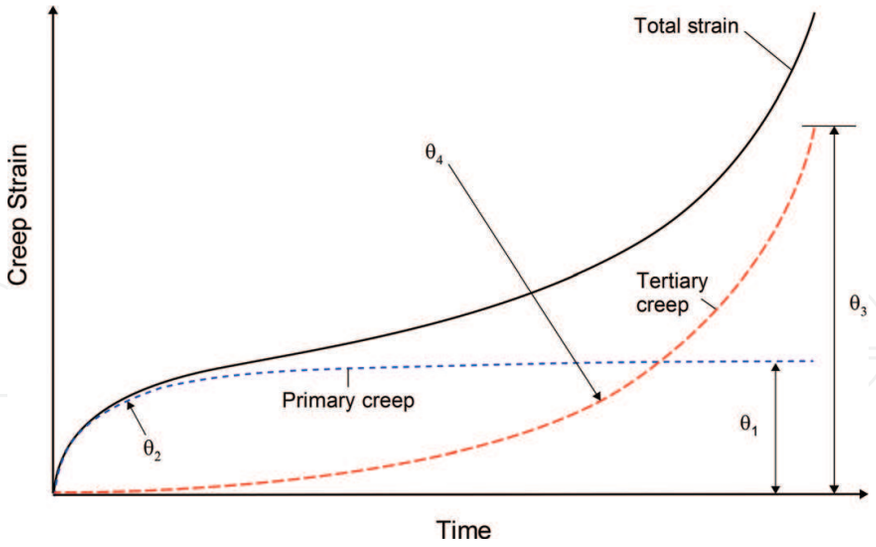

Figure 3. Schematic representation of a creep curve represented by Eq. (7), showing primary and tertiary regions.

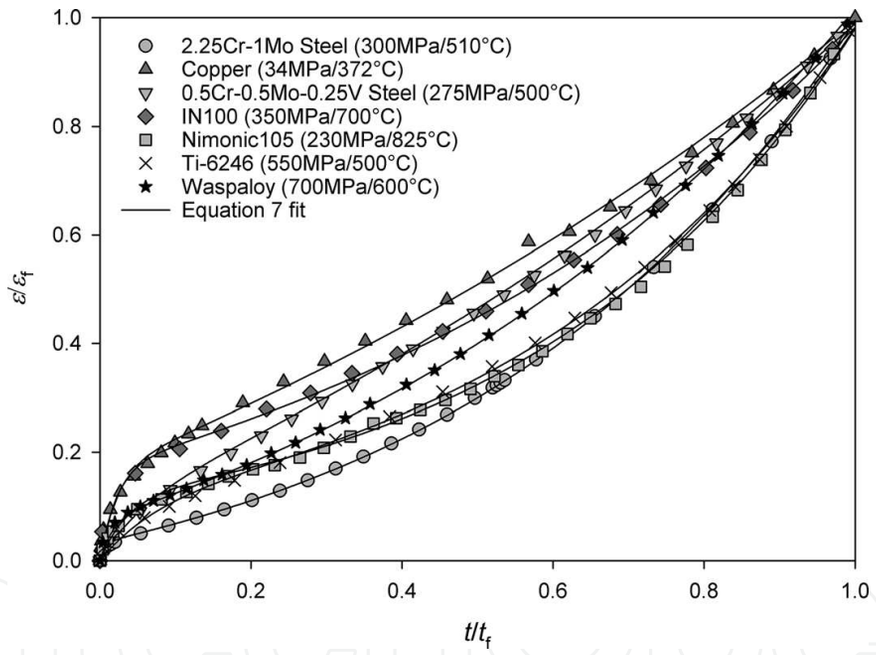

Figure 4. Examples of creep curves represented by the theta-projection method (Eq. (7)).

$$\ln(\theta_k)_h = a_k + b_k\sigma_h + c_k T_h + d_k\sigma_h T_h, \qquad k = 1\text{–}4 \tag{9}$$

where a_k, b_k, c_k and d_k (k = 1–4) are obtained by linear regression. This empirical approach interpolates the θ-coefficients well, however produces unrealistic values when extrapolating to applied conditions beyond existing experimental data. Poor extrapolation is problematic when evaluating the creep behaviour of complex engineering components using finite element analysis (FEA) since some regions of the components may have values of σ and T that do not correspond to those tested through uniaxial creep tests [10]. An alternative approach is to use a

power law expression to relate θ_{1-4} to σ and an Arrhenius expression to account for temperature effects. For the titanium aluminide alloy Ti-45Al-2Mn-2Nb the stress was normalised against temperature compensated tensile strength, σ_{TS}, which was sufficient to account for temperature effects for θ_1 and θ_3 [20]. The equations used to relate θ_{1-4}. To applied test conditions are

$$\theta_1 = A_1\left(\frac{\sigma}{\sigma_{TS}}\right)^{n_1} \tag{10}$$

$$\theta_2 = A_2\left(\frac{\sigma}{\sigma_{TS}}\right)^{n_2}\exp\left(\frac{-Q_2^*}{RT}\right) \tag{11}$$

$$\theta_3 = A_3\left(\frac{\sigma}{\sigma_{TS}}\right)^{n_3} \tag{12}$$

$$\theta_4 = A_4\left(\frac{\sigma}{\sigma_{TS}}\right)^{n_4}\exp\left(\frac{-Q_4^*}{RT}\right) \tag{13}$$

where Q_k^*, A_k and n_k (k = 1, 4) are determined from θ-coefficents obtained using Eq. (8). The parameters of Eqs. (10) and (11) are determined from the gradients and intercepts of linear lines of best fit from plots of $\ln(\theta_1)$ and $\ln(\theta_3)$ against $\ln(\sigma/\sigma_{TS})$ respectively. θ_2 and θ_4 display more dependence on temperature and are evaluated from plots of $\ln\left[\theta_2\exp\left(Q_2^*/RT\right)\right]$ and $\ln\left[\theta_4\exp\left(Q_4^*/RT\right)\right]$ against $\ln(\sigma/\sigma_{TS})$ respectively. Since, stress is normalised using temperature dependent tensile strength Q_2^* and Q_4^* are lower than values for activation energy evaluated against σ alone. A common activation energy of 330 KJmol^{-1} was found to apply to both Q_2^* and Q_4^*, a value similar to the measured interdiffusion coefficient for γ-TiAl [20] indicating that this mechanism plays an important role in creep of these types of alloy. The relationship of the θ-coefficients with respect to stress and temperature for Ti-45Al-2Mn-2Nb can be seen in **Figure 5**.

An alternative approach to the θ-projection method is a true stress model proposed by Wu et al. [19]. This method relates total strain, ε to time, t, by

$$\varepsilon = \varepsilon_0 + \varepsilon_p\left[1 - \exp\left(-\frac{t}{t_{tr}}\right)\right] + \frac{1}{M'}\left[\exp(M'kt) - 1\right] \tag{14}$$

where ε_0 is the instantaneous strain, ε_p represents the magnitude of primary creep and t_{tr} is the transient time. M' and k are related to the calculated rates of dislocation glide, climb and grain boundary sliding. This equation has a similar form to Eq. (7) where $\theta_1 = \varepsilon_p$, $\theta_2 = 1/t_{tr}$, $\theta_3 = 1/M'$ and $\theta_4 = M'k$. M' and k are related to calculated rates of dislocation glide, climb and grain boundary sliding obtained from experimental creep curves.

2.2. Hardening methods

Various methods to predict creep curves and hence creep rates during uniaxial creep have been proposed, however, to predict creep behaviour in engineering components using FEA, a

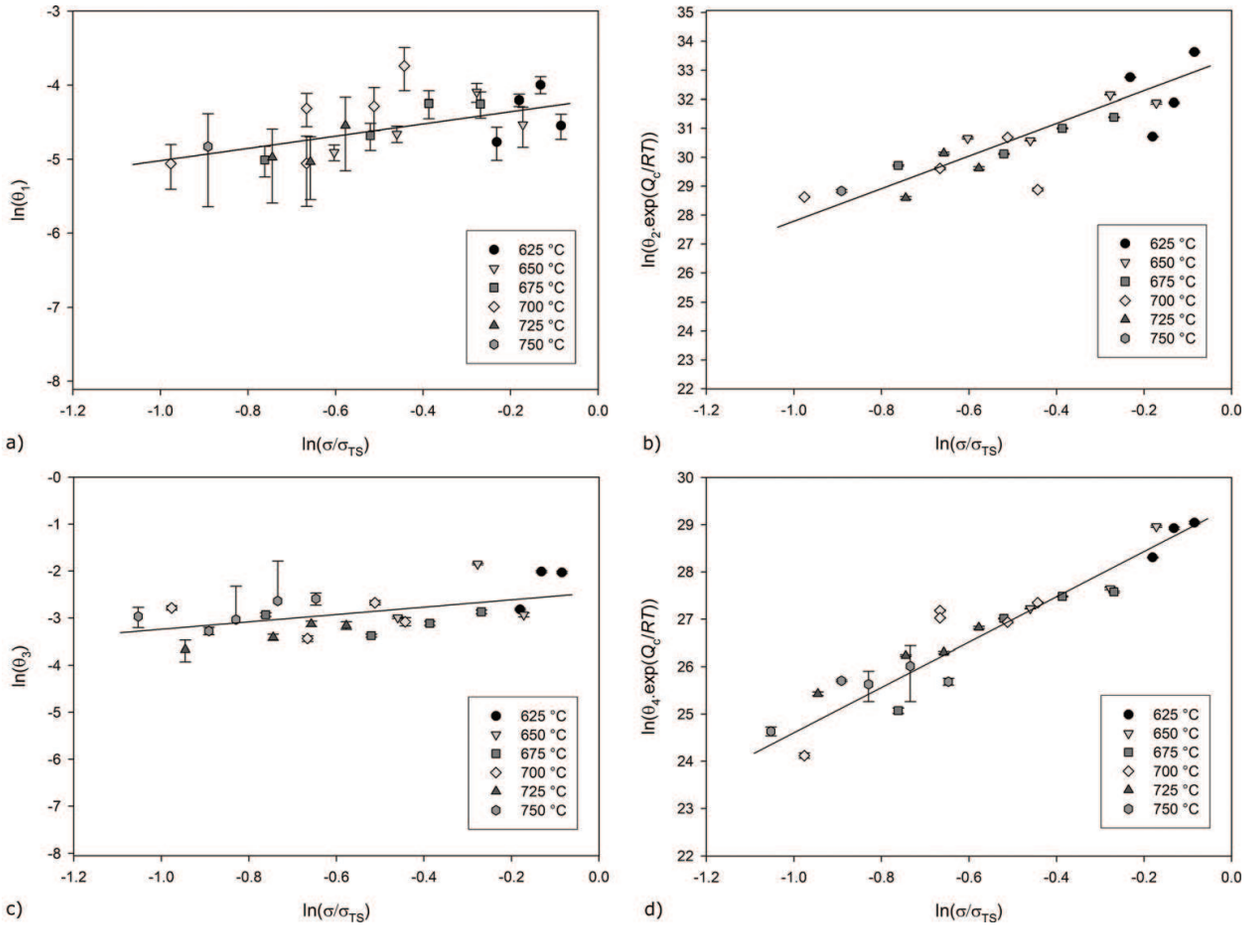

Figure 5. The stress and temperature dependence of: (a) θ_1; (b) θ_2; (c) θ_3 and (d) θ_4 for the titanium aluminide alloy Ti-45Al-2Mn-2Nb [20].

suitable hardening model is required. During uniaxial constant stress creep, creep rate, $\dot{\varepsilon}_c$, is dependent on applied stress, temperature and the time and/or strain for which the conditions have been applied.

$$\dot{\varepsilon}_c = f(\sigma, T, t) \tag{15}$$

However, in real engineering situations, the stress and/or temperature may change, resulting in the calculation of a different creep curve. Therefore, creep behaviour is now dependent on the position on the creep curve at new applied conditions and therefore more information is required to calculate creep rate. The simplest case is to consider that the new creep rate relates to the current creep time on the new curve (time-based hardening). This method, although easy to implement, fails to accurately account for strain rate changes for all but minor changes in applied conditions. For large changes in creep conditions, the shape of the creep curve changes significantly resulting in poor predictions. An alternative method is to relate creep rate to the applied conditions and creep strain history (strain-based creep hardening). For this case, the strain rate is calculated at the point on a creep curve which relates to the current total creep strain. This method, although more accurate that time-based hardening, produces inaccuracies when creep conditions change from primary creep dominated to tertiary creep dominated.

To address the shortcomings of these methods, a life-fraction hardening method is often used. This method uses an effective time based on t/t_F where t_F is the creep rupture life for the applied stress and temperature. A graphical representation of these hardening methods is given in **Figure 6**.

An alternative method of creep hardening is to base creep rate on the applied conditions and various material state variables

$$\dot{\varepsilon} = \Phi(\sigma, T, \xi_1, \xi_2, \ldots, \xi_\alpha, \ldots, \xi_n) \tag{16}$$

Where ξ_α ($\alpha = 1$, n) are internal material state variables, each dependent on the loading history of the material. Evans [17], proposed that creep rate is dependent internal state variables representing dislocation hardening (H), recovery (R) and damage (W):

$$\dot{\varepsilon} = \dot{\bar{\varepsilon}}_0(1 + H + R + W) \tag{17}$$

where $\dot{\bar{\varepsilon}}_0$ is the initial effective creep rate of the virgin material. Each of these state variables represents the many mechanisms which control creep rate. These variables are related to both the strain and time history by the proportionality constants $\widehat{H}$, $\widehat{R}$ and $\widehat{W}$, such that:

$$\dot{H} = -\widehat{H}\dot{\varepsilon} \tag{18}$$

$$\dot{R} = \widehat{R} \tag{19}$$

$$\dot{W} = \widehat{W}\dot{\varepsilon} \tag{20}$$

The initial effective creep rate and proportionality constants can be related to applied condition using the θ coefficients from Eq. (7),

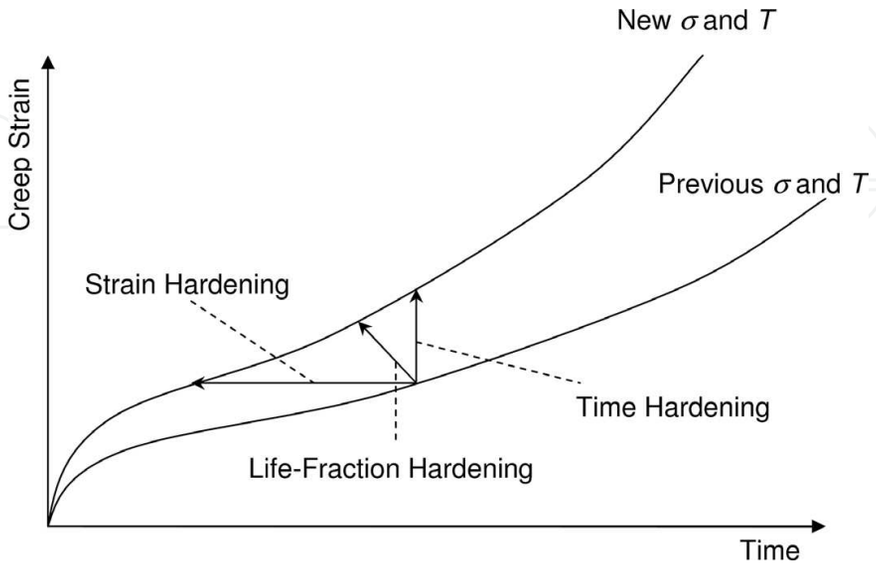

Figure 6. Schematic representation of time, strain and life-fraction hardening.

$$\dot{\bar{\varepsilon}}_0 = \theta_1\theta_2 + \theta_3\theta_4 \tag{21}$$

$$\widehat{H} = \frac{\theta_2}{\theta_1\theta_2 + \theta_3\theta_4} \tag{22}$$

$$\widehat{R} = \frac{\theta_2\theta_3\theta_4}{\theta_1\theta_2 + \theta_3\theta_4} \tag{23}$$

$$\widehat{W} = \frac{1}{\theta_3} \tag{24}$$

If damage is assumed to be purely a tertiary process, the effective creep rate, $\dot{\bar{\varepsilon}}$, can be calculated from Eqs. (21)–(24) using [17]:

$$\dot{\bar{\varepsilon}} = \dot{\bar{\varepsilon}}_0\left(\frac{1 + H + R + \widehat{R}}{\widehat{H}\dot{\bar{\varepsilon}}_0}W\right) \tag{25}$$

For virgin material, H, R and W are equal to zero, however as creep continues their values are updated for each time increment, ∂t, using [17]:

$$H_{i+1} = H_i - \widehat{H}\dot{\bar{\varepsilon}}_0(1 + H_i + R_i)\partial t \tag{26}$$

$$R_{i+1} = R_i + \widehat{R}\partial t \tag{27}$$

$$W_{i+1} = W_i + \frac{\widehat{W}\widehat{R}}{\widehat{H}}(1 + W_i)\partial t \tag{28}$$

Transient uniaxial creep tests have been used to test the ability of different hardening methods to predict creep at non-constant stress and temperature for the nickel based superalloy, Waspaloy [8]. These creep tests applied temperature and stress which changed between two sets of conditions, one at high stress and low temperature, the other at low stress and high temperature, with both sets of conditions predicted to give similar lives approximately 10 days. The applied conditions were changed every 24 hours with a 1 hour transition period to allow sufficient time for the temperature to change, during which the stress was held at the lower level of the two conditions. **Figure 7** shows the creep rates observed from a transient creep test in which the temperature was changed from 600 to 750°C with applied stresses of 880 MPa and 390 MPa respectively, along with the test data for the equivalent isothermal constant stress creep tests. Immediately after each applied condition change, it can be seen that the creep rates are initially high before decreasing in what appears to be regions of 'pseudo' primary creep. In general, the creep rates observed during transient creep are higher than those observed for isothermal constant stress creep. The creep rates for the test at 600°C with an applied load of 880 MPa display a large proportion of primary creep, shown by the initially high creep rate followed by a gradual decrease, whereas the test at 750°C and 390 MPa is dominated by tertiary creep, with a minimum creep rate achieved after only 10% of life.

Eq. (8) was used to numerically describe the isothermal constant stress creep data to allow different hardening methods to be evaluated against transient creep rates (**Figure 8**). Time

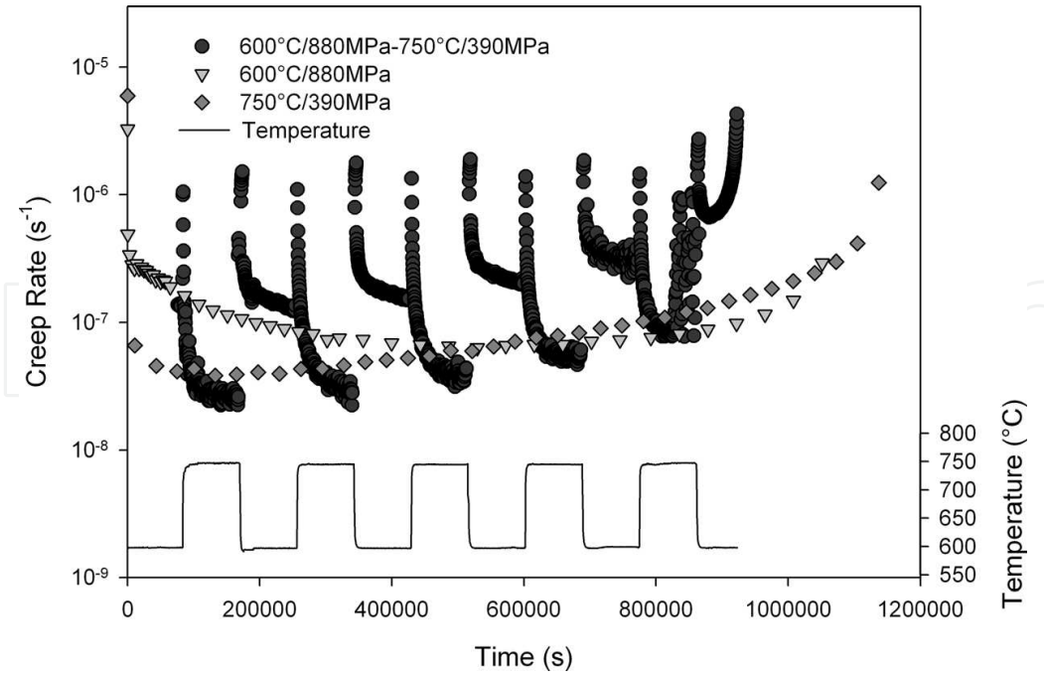

Figure 7. Creep rates obtained from transient and isothermal constant stress creep tests for Waspaloy at 600°C/880 MPa and 750°C/390 MPa [8].

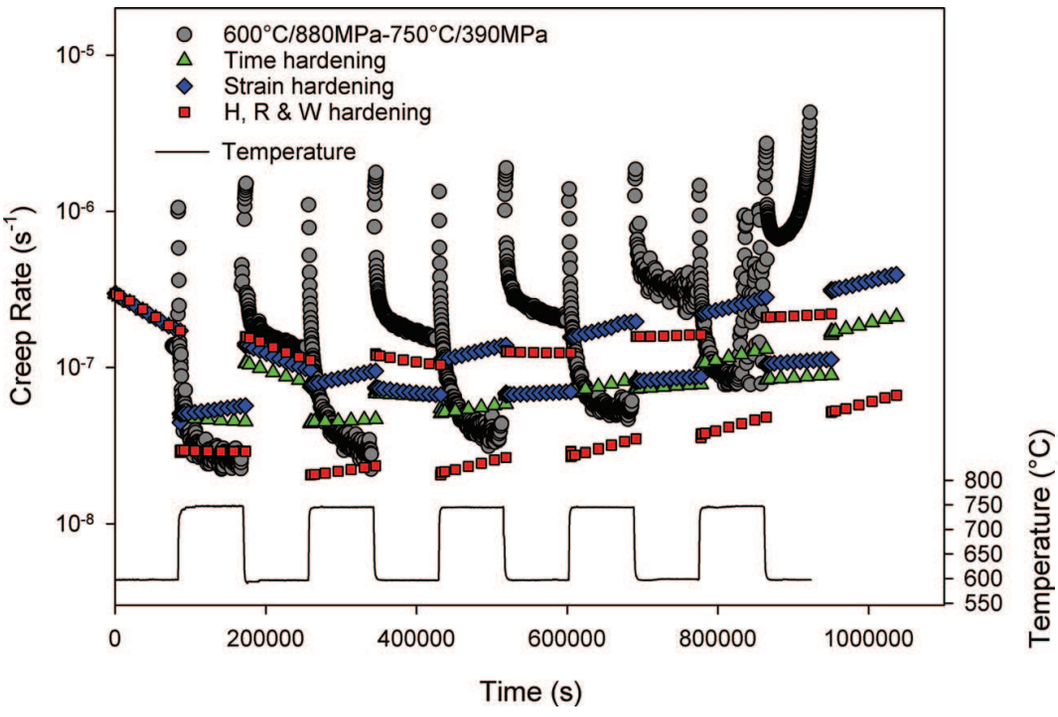

Figure 8. Creep transient creep behaviour for Waspaloy with predicted creep rates using time-hardening, strain hardening and a hardening model based on internal state variables.

hardening strain hardening and the hardening method based on internal state variables all predict the first cycle well, however for subsequent cycles the predictions using time and strain based hardening fail to predict the overall trend in creep rate, as well as the local peaks in rate

after each load change. In this case, since the predicted rupture lives at each set of conditions is similar, life-fraction hardening would display a similar trend to time-based hardening. The creep rates predicted for a hardening method based on internal state variables describes the trend in rate more accurately but also fails to predict the 'pseudo' primary creep at the beginning of each cycle.

At both sets of creep conditions, creep occurs by diffusion controlled movement of dislocations, however, the dominant mechanism by which this occurs is varies between the high-stress/low-temperature and low-stress/high-temperature cases. At the high stress condition, the stress exceeds the yield point resulting in the formation of new dislocations. This leads to higher dislocations in the material at high stress than in the low stress material which only contains dislocations present after forming. Furthermore, at the higher temperature state, more thermal energy is available for diffusion controlled creep mechanisms such as climb. Whereas at low temperatures but higher stresses, precipitation cutting becomes more dominant. Therefore, when changing between two sets of creep conditions, the creep rate is dependent on the loading history of the material.

3. Creep damage and rupture

For simple uniaxial models failure can be creep rupture times may be predicted using simple equations such as those proposed to Norton [1], Larson and Miller [2]. However, for cases where the stress and temperature evolve over time a different approach is required. Creep damage models allow the accumulation of damage to be predicted regardless of applied conditions. Kachanov [21] proposed that the increase in creep rate during tertiary creep could be related to an increase in stress caused by a decrease effective cross sectional area due to the nucleation and growth of grain boundary cavities and triple point cracking. Later, Rabotnov [22] extended this idea by introducing a continuum damage parameter, ω, to represent this decrease in effective cross section. Leckie and Hayhurst [23] generalised this approach and Othman and Hayhurst [24] extended it to include the effects of primary creep. The constitutive model based on the θ-projection method includes internal state variables for dislocation hardening, H, recovery, R, and creep damage, W. Of particular interest to the case of creep rupture is W which represents the sum of all damage processes that occur during tertiary creep. W is zero for virgin material and increases as creep continues. Failure is predicted when this parameter exceeds a critical value, W_F. The value of W_F can be obtained from experimentally obtained creep tests using

$$W_F = \frac{1}{\theta_3}\left[\varepsilon_F - \theta_1\left(1 - e^{-\theta_2 t_F}\right)\right] \tag{29}$$

where ε_F is the creep strain at failure and θ_{1-3} are obtain using Eq. (8). W_F must then be related to applied creep conditions. For the γ-TiAl alloy, Ti-45Al-2Mn-2Nb, the following expression was found to represent the stress rupture data well

$$W_F = c + ln\left(\frac{\sigma}{\sigma_{TS}}\right)K \tag{30}$$

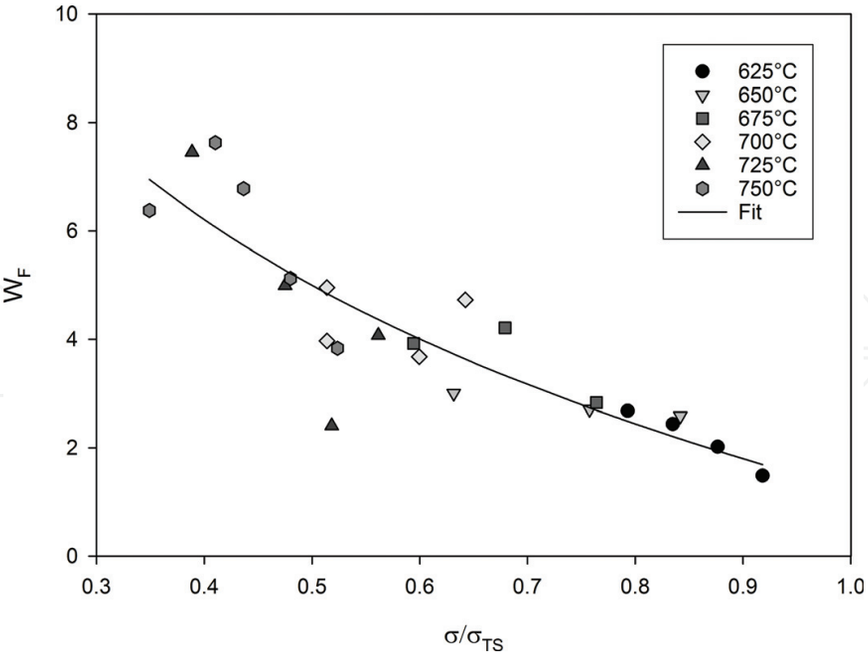

Figure 9. The dependence of W_F on applied creep conditions for Ti-45Al-2Mn-2Nb.

where σ_{TS} is the temperature dependent ultimate tensile strength and c and K are derived from experimental data by plotting W_F against $\ln(\sigma/\sigma_{TS})$. A plot of critical damage against applied stress is given in **Figure 9**. Since this data is derived from uniaxial test data, the applied stress, σ, may represent the von-Mises stress, $\overline{\sigma}$, or the maximum principle stress, σ_1.

Where multiaxial creep data is available, the dependence of W and W_F on σ_1 can be evaluated. For Waspaloy, W_F, can be related to applied stress using:

$$W_F = 237.3 \exp\left[-5.828\left(\frac{\sigma_1}{\sigma_{TS}}\right)\right] \tag{31}$$

where σ_{TS} is the temperature dependent tensile strength [17]. For other alloys such as the titanium alloy Ti6246, less dependence on loading direction was found and W_F can be related to $\overline{\sigma}$ [10].

4. Finite element analysis

Once suitable methods to interpolate creep curves for any given condition and suitable hardening models have been derived, it is possible to compile models for use in finite element analyses (FEA). The constitutive model based on the θ-project method [17] and the Wilshire creep curve method [13] have both been incorporated into FEA as user defined subroutines for the commercially available software Abaqus [10]. In order to evaluate creep deformation and damage, the user must define the magnitude of creep strain accumulated at each time step, based on stress, temperature and any user defined state variables. Furthermore, if implicit integration is used, the derivative of the creep strain increment with respect to stress must also

be defined. User defined state variables such as those used to represent internal material damage (W) must also be evaluated. These models have been used to predict creep behaviour in various engineering applications [10, 25].

4.1. Stress relaxation

An application to consider is stress relaxation due to creep. This can be predicted using a simple single element finite element model with a prescribed displacement boundary condition. **Figure 10** shows a good correlation of the predicted and experimentally obtained results of a two stage stress relaxation experiment in the nickel based superalloy Alloy720Li using a model based on the strain hardening formulation of the Wilshire creep curve extrapolation method.

4.2. Notched bars

The value of FEA comes from its ability to predict mechanical behaviour in engineering components with complex geometries. Components such as those found in gas turbine aeroengines operate at high temperatures for extended periods of time and any geometric feature of the component that concentrates stress will exhibit higher creep rates than surrounding regions resulting in a redistribution of stress. Accurate predictions of this stress redistribution are particularly important for cases where component lives are influenced by fatigue as the stress field affects subsequent fatigue calculations. Furthermore, creep failure can initiate in subsurface locations due to a combination of stress redistribution and subsurface damage [10].

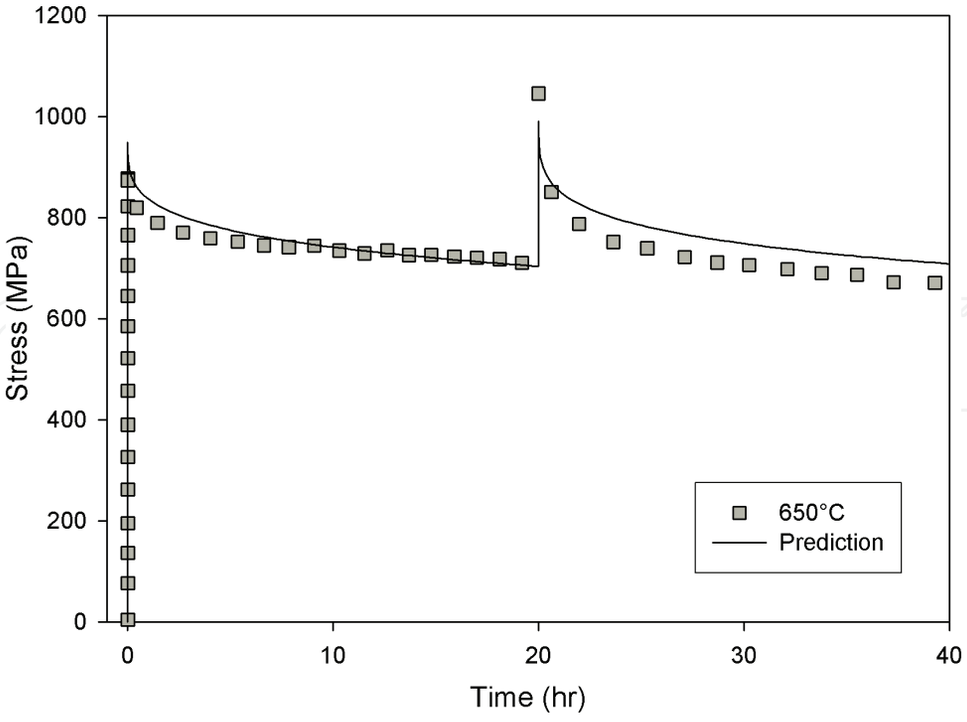

Figure 10. Uniaxial stress relaxation in Alloy720Li at 650°C with prediction using the Wilshire creep curve extrapolation method (Eqs. (5) and (6)) with strain-based hardening.

Predictions of stress redistribution in a Waspaloy round circumferentially notched bar after 1000 s of creep deformation using the θ-projection method can be seen in **Figure 11**.

The constitutive model based on the θ-projection technique contains material state variables for dislocation hardening, H, recovery, R, and damage, W. The latter allows for predictions of material failure as W exceeds a critical value W_F. In this model, material failure is simulated by reducing element stiffness when $W/W_F > 1$. In Abaqus, this is achieved by using a field variable dependent elastic modulus which decreases by an order of magnitude as the failure criteria is exceeded. Using this method, predictions of creep rupture can be made for cases when the stress and/or temperature is not constant. Predictions of the rupture times of both round and v-shaped circumferentially notched Waspaloy creep specimens correlate well with experimental data and predicted fracture paths are consistent with those observed experimentally [17]. Due to the dependence of W_F on stress triaxiality, different paths of failure are observed for different shaped notched with more diffuse damage occurring with lower stress intensities (K_T). Predicted creep rupture paths in round and v-shaped circumferentially notched Waspaloy specimens are shown in **Figure 12**.

4.3. Small punch creep

The small punch creep test is often used to characterise the mechanical properties of materials where only small quantities exist, such as during novel alloy development or for remnant life assessment [25–27]. The test consists of applying load to the centre of a small disc of material, typically 0.5 mm thick with a diameter of 9.5 mm, using a hemispherical punch. Punch load and displacement are then related to uniaxial stress and strain using conversion factor, k_{SP}. During small punch creep, the stress state evolves as punch displacement increases and therefore finite element analyses can provide useful information about the accumulation of creep strain and damage. Furthermore, by comparing the fracture path to the predicted stress, a greater understanding of the role of the stress state on creep rupture can be obtained.

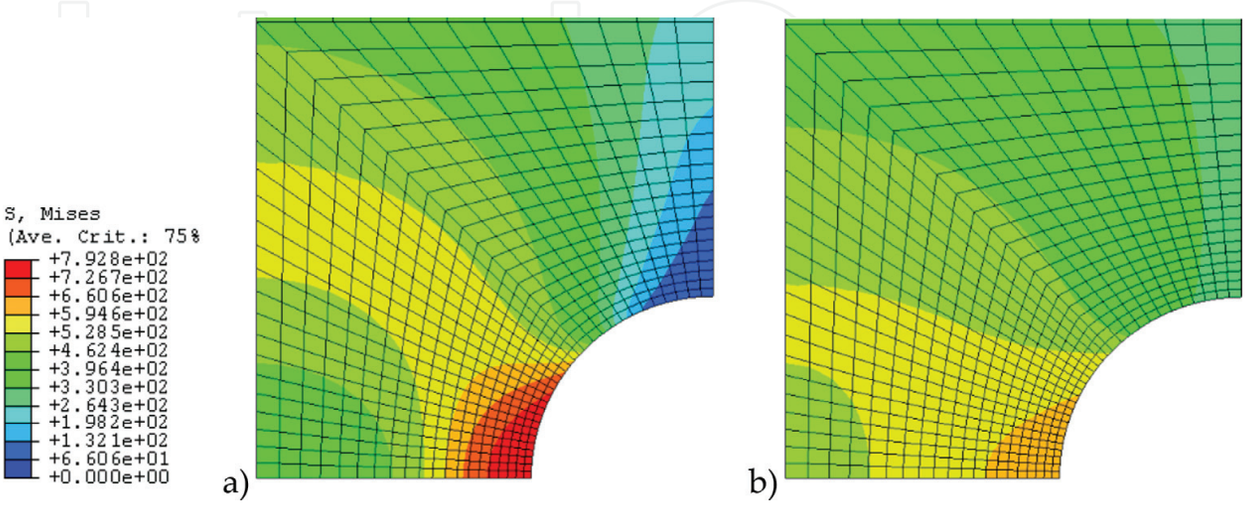

Figure 11. Stress distribution in a Waspaloy round circumferentially notched bar at (a) 0 s and (b) 1000 s at 650°C with an applied stress equating to 800 MPa across the specimen neck.

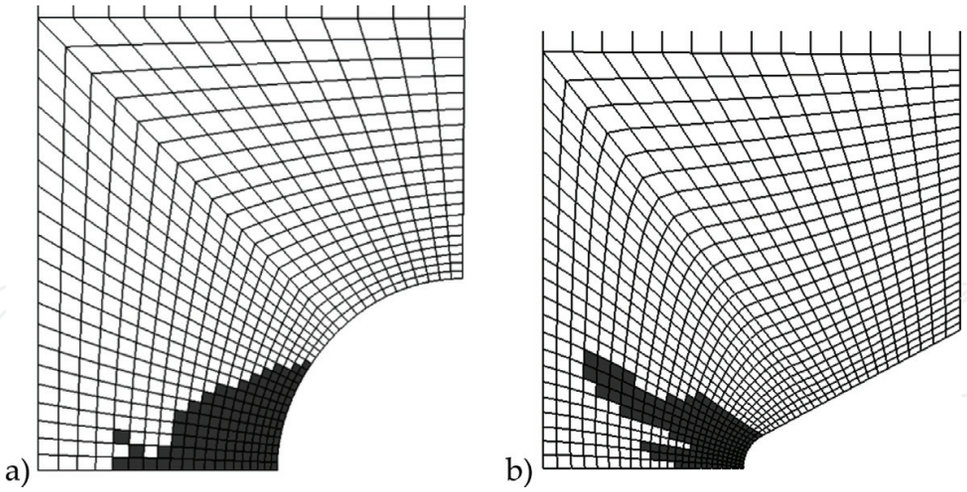

Figure 12. Predicted damage in a Waspaloy (a) round notched (K_T = 1.4) and (b) v-shaped notched (K_T = 2.234) test specimens.

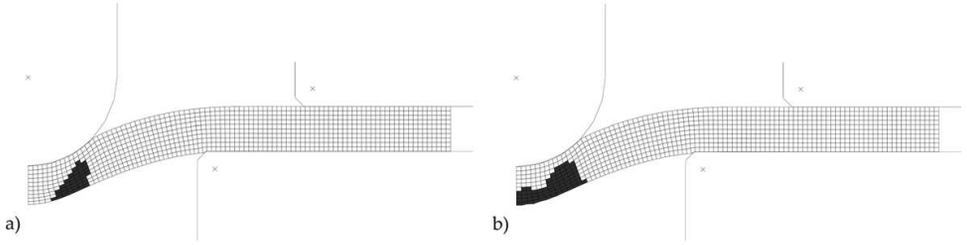

Figure 13. Predicted damage in a TiAl small punch test with damage based on (a) von-Mises stress and (b) maximum principle stress [25].

Predictions of the small punch creep behaviour of Ti-45Al-2Mn-2Nb have been made using the constitutive model based on the θ-projection method (**Figure 13**).

4.4. High-temperature fatigue

The effects of creep in engineering components that are exposed to cyclic loading at high temperatures cannot be ignored. A fatigue crack propagating through material exhibiting creep damage will advance more rapidly as creep cavities and microvoids provide a preferential path for growth. In this case fatigue lives are negatively affected by creep damage and cracks propagate along grain boundaries (intergranular). However, redistribution of stress due to creep can reduce stress at stress concentration features such as cracks and notches, reducing the driving force for crack propagation, hence increasing fatigue lives. This has been clearly shown in the titanium alloy Ti-6Al-4V whereby increasing the temperature from 450 to 500°C increases the fatigue lives of notched specimens, whereas a further increase to 550°C has a negative effect on life [28]. Therefore, during high temperature fatigue, component life is a dependent on time-dependent (creep) and time-independent (fatigue) damage mechanisms. FEA can be used to predict stress relaxation around notches and cracks, as well as to evaluate damage ahead of an advancing crack. Using a quasi-static model, the accumulation of creep deformation and damage ahead of an advancing fatigue crack in the titanium alloy, Ti-6246 has been predicted (**Figure 14**) [10].

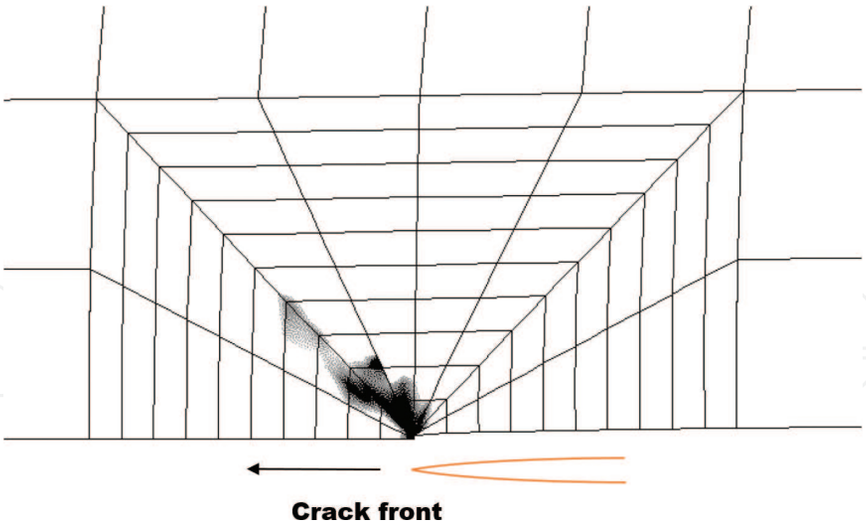

Figure 14. Predicted creep damage around the crack tip after 6×10^4 s at 773 K (R = 0.1, ΔK = 22) in Ti-6246 [10].

5. Conclusions

Although simple single point prediction methods can be useful for certain applications, accurate predictions of the mechanical response of some engineering components that operate at elevated temperatures require creep models that predict the full shape of the creep curve. These models, implemented in FEA have been used to predict creep behaviour in cases where stress and/or temperature are not constant, such as during stress relaxation. Furthermore, attempts have been made to relate model parameters to observed micromechanical behaviour. Creep damage models have been used to provide useful predictions of creep life which can be used to evaluate time dependent damage during other load cases, such as during high temperature fatigue and thermo-mechanical fatigue.

Author details

William Harrison*, Mark Whittaker and Veronica Gray

*Address all correspondence to: w.harrison@swansea.ac.uk

Swansea University, Swansea, Wales, UK

References

[1] Norton FH. The Creep of Steels at High Temperatures. New York: McGraw-Hill; 1929. 112 p

[2] Larson FR, Miller J. A time-temperature relationship for rupture and creep stresses. Trans. ASME. 1952;**74**:765-775

[3] Williams SJ, Bache MR, Wilshire B. 25 Year Perspective Recent developments in analysis of high temperature creep and creep fracture behaviour. Materials Science and Technology. 2010;**26**(11):1332-1337

[4] Wilshire B, Battenbough AJ. Creep and fracture of polycrystalline copper. Materials Science and Engineering A. 2007;**443**:156-166

[5] Whittaker MT, Harrison WJ, Lancaster RJ, Williams S. An analysis of modern creep lifing methodologies in the titanium alloy Ti6-4. Materials Science and Engineering: A. 2013; **577**:114-119

[6] Abdallah Z, Gray V, Whittaker M, Perkins K. A critical analysis of the conventionally employed creep lifing methods. Materials. 2014;**7**(5):3371-3398

[7] Monkman FC, Grant NJ. An empirical relationship between rupture life and minimum creep rate. In: Grant NJ, Mullendore AW, editors. Deformation and Fracture at Elevated Temperatures. Boston: MIT Press; 1965

[8] Harrison WJ, Whittaker MT, Deen C. Creep behaviour of Waspaloy under non-constant stress and temperature. Materials Research Innovations. 2013;**17**(5):323-326

[9] Whittaker M, Lancaster R, Harrison W, Pretty C, Williams S. An empirical approach to correlating thermo-mechanical fatigue behaviour of a polycrystalline Ni-base superalloy. Materials. 2013;**6**(11):5275-5290

[10] Harrison W. Creep modelling of Ti6246 and Waspaloy using ABAQUS [thesis]. UK: University of Wales Swansea; 2007

[11] Gray V, Whittaker M. Development and assessment of a new empirical model for predicting full creep curves. Materials. 2015;**8**(7):4582-4592

[12] Abdallah Z, Perkins K, Williams S. Advances in the Wilshire extrapolation technique—Full creep curve representation for the aerospace alloy Titanium 834. Materials Science and Engineering: A. 2012;**550**:176-182

[13] Harrison W, Whittaker M, Williams S. Recent advances in creep modelling of the nickel base superalloy, alloy 720Li. Materials. 2013;**6**(3):1118-1137

[14] Whittaker MT, Wilshire B. Creep and creep fracture of 2.25Cr-1W steels (Grade 23). Materials Science and Engineering A. 2010;**527**(18):4932-4938

[15] Whittaker MT, Harrison WJ, Deen C, Rae C, Williams S. Creep deformation by dislocation movement in Waspaloy. Materials. 2017;**10**(61):1-14

[16] Evans RW, Parker JD, Wilshire B. An extrapolation procedure for long-term creep strain and creep life prediction, with special reference to 0.5Cr0.5Mo0.25V ferritic steels. In: Wilshire B, Owen DRJ, editors. Recent Advances in Creep and Fracture of Engineering Materials and Structures. Swansea: Pineridge Press; 1982. p. 135

[17] Evans RW. A constitutive model for the high-temperature creep of particle-hardened alloys based on the θ projection method. Proceedings of the Royal Society of London A: Mathematical, Physical and Engineering Sciences. 2000;**456**(1996):835-868

[18] Dyson BE, McLean M. Microstructural evolution and its effects on the creep performance of high temperature alloys. In: Microstructural Stability of Creep Resistant Alloys for High Temperature Plant Applications. Institution of Metals, London; 1998, pp. 371-393

[19] Wu X, Williams S, Gong D. A true-stress creep model based on deformation mechanisms for polycrystalline materials. Journal of Materials Engineering and Performance. 2012;**21** (11):2255-2262

[20] Harrison W, Abdallah Z, Whittaker M. A model for creep and creep damage in the γ-titanium aluminide Ti-45Al-2Mn-2Nb. Materials. 2014 Mar 14;**7**(3):2194-2209

[21] Kachanov LM. Rupture time under creep conditions. International journal of fracture. 1999 Apr 1;**97**(1-4):11-18

[22] Rabotnov YN. Creep Problems in Structural Members. Amsterdam: North-Holland; 1969

[23] Leckie FA, Hayhurst DR. Constitutive equations for creep rupture. Acta Metallurgica. 1977;**25**(9):1059-1070

[24] Othman AM, Hayhurst DR. Multi-axial creep rupture of a model structure using a two parameter material model. International Journal of Mechanical Sciences. 1990;**32**(1):35-48

[25] Lancaster RJ, Harrison WJ, Norton G. An analysis of small punch creep behaviour in the γ titanium aluminide Ti–45Al–2Mn–2Nb. Materials Science and Engineering: A. 2015;**626**: 263-274

[26] Kobayashi KI, Kajihara I, Koyama H, Stratford GC. Deformation and fracture mode during small punch creep tests. Journal of Solid Mechanics and Materials Engineering. 2010;**4**(1):75-86

[27] Blagoeva D, Li YZ, Hurst RC. Qualification of P91 welds through small punch creep testing. Journal of Nuclear Materials. 2011;**409**(2):124-130

[28] Whittaker MT, Harrison W, Hurley PJ, Williams S. Modelling the behaviour of titanium alloys at high temperature for gas turbine applications. Materials Science and Engineering: A. 2010;**527**(16):4365-4372